

Identification, Structure, and Spectroscopy of Neutral Vanadium Oxide Clusters

Yoshiyuki Matsuda and Elliot R. Bernstein*

Department of Chemistry, Colorado State University, Fort Collins, Colorado 80523-1872

Received: November 12, 2004; In Final Form: February 8, 2005

Neutral vanadium oxide clusters are studied by photoionization time-of-flight (TOF) mass spectroscopy, electronic spectroscopy, and density functional theory (DFT) calculations. Mass spectra of vanadium oxide clusters are observed by photoionization with lasers of three different wavelengths: 118, 193, and 355 nm. Mechanisms of 118 nm single photon ionization and 193 and 355 nm multiphoton ionization/fragmentation of vanadium oxide clusters are discussed on the basis of observed mass spectral patterns and line widths of the mass spectral features. Only the 118 nm laser light can ionize vanadium oxide neutral species by single photon ionization without fragmentation. The stable vanadium oxide neutral clusters under saturated oxygen growth conditions are found to be of the form $(\text{VO}_2)_x(\text{V}_2\text{O}_5)_y$. Structures of the first few members of this series of clusters are determined through high level DFT calculations. Fragmentation of this series of clusters through 355 and 193 nm multiphoton ionization processes is discussed in light of these calculated structures. The $\tilde{\text{B}}^2\text{B}_2 \leftarrow \tilde{\text{X}}^2\text{A}_1$ transition is observed for the VO_2 neutral species, and ν_1 and ν_2 vibrations are assigned for both electronic states. From this spectrum, the VO_2 rotational and vibrational temperatures are found to be ~ 50 and ~ 700 K, respectively.

I. Introduction

Vanadium oxide catalysts are found throughout the chemical industry and synthesis laboratories. Nonetheless, the microscopic properties of specific local catalytic sites and the mechanism for catalytic activity of vanadium oxide catalysts remain unknown. The electronic and geometric structures of vanadium oxide gas phase clusters can correspond to condensed phase surface and/or defect structures, and thus, such clusters can have properties and behavior that relate or correspond to condensed phase chemical and physical phenomena. This local approach to condensed phase modeling was first articulated by Mutttert¹ and has since been explored by a number of other research groups.²

Numerous studies of ionic vanadium oxide clusters (V_mO_n^\pm) have been reported.^{3–13} Theoretical studies of the structures for ionic vanadium oxide clusters have been accomplished,³ and these structures have been employed to explore cluster ion reactivity.^{3e} Experimentally, extensive mass spectroscopic and reaction studies have been reported for vanadium and vanadium oxide cations by the groups of Armentrout,⁴ Castleman,⁵ and Schwarz.⁶ Photoelectron, zero electron kinetic energy (ZEKE), electronic, and infrared spectroscopic studies have been performed for ionic clusters by the groups of Hackett,⁷ Kaya,⁸ Leopold,⁹ Lineberger,¹⁰ Wang,¹¹ Kondow,¹² and Meijer.¹³

Electronic spectroscopy of neutral metal oxide clusters is performed mainly by photoelectron spectroscopy for cluster anions in order to associate a spectrum with a given size cluster. A major difficulty for electronic spectroscopy of neutral clusters relates to the coexistence of many clusters in the gas phase simultaneously; a mass selective spectroscopic technique is required for a positive identification of the species carrying the observed spectrum. Cluster ionization is thereby required for the spectroscopic observation, but cluster fragmentation (loss

of mass selectivity) is always a question. Nonetheless, electronic spectra for VO and V_2 have been reported.¹⁴

Mass spectrometric studies of neutral vanadium oxide clusters detected with photoionization are reported by Riley and co-workers¹⁵ and Bernstein and co-workers.¹⁶ In the former study, pure neutral V_n clusters are produced by laser ablation and expansion as a first step. These clusters are then passed into a flow tube reactor with O_2 gas, and neutral V_mO_n clusters are generated. The V_mO_n clusters are ionized by either a 193 (ArF), 248 (KrF), or 308 (XeCl) nm laser and detected and identified by time-of-flight (TOF) mass spectroscopy. In the latter study, neutral vanadium oxide clusters are produced by mixing the ablated metal plasma with an O_2 (0.1–6%)/He (99.9–94%) mixture directly and expanding the subsequent mixture into a vacuum system. Neutral clusters in this experiment are ionized by low intensity 193 nm radiation; the observed mass spectra look quite similar to those of ref 15. Fielicke et al.¹⁷ report infrared multiphoton dissociation spectra for vanadium oxide/ethylene cation clusters. They analyze fragmentation pathways through the wavelength dependence of the IR spectrum of ethylene for the observed fragment mass peaks.

Cluster fragmentation or loss of mass information during the ionization process required for detection is the motivating factor for the use of covariance mapping^{16,18} analysis of mass spectra. A covariance mapping analysis of vanadium oxide mass spectra (193 nm ionization) shows a positive correlation between mass spectral features, implying, according to ref 16, that the observed V_mO_n^+ clusters are related through a growth mechanism. In order not to lose information on the neutral cluster distribution, we have recently applied low energy/pulse ($\sim 1 \mu\text{J}$), high energy/photon (10.5 eV, 118 nm) ionization for determination of the neutral cluster distribution of metal oxides.¹⁹ The 10.5 eV photons have sufficient energy to ionize almost all neutral metal oxide clusters.^{19,20} (Note, however, that according to our calculations, VO_3 and VO_4 , at ionization energies of ~ 11.5 eV, may be exceptions to this generalization.)

* Corresponding author. E-mail: erb@lamar.colostate.edu. Phone: 970-491-6347. Fax: 970-491-1801.

Calculations have also been pursued for neutral vanadium oxide clusters at various levels of density functional^{3a–d,21a} and *ab initio* theory.^{3c,d,21b} Additionally, simulations of cluster reactivity and surface reactions have also been reported for this system.²² V_2O_4 structures are reported by Pykavy et al.^{3d} at the MR-ACPF/cc-pVQZ and B3LYP/cc-pVQZ levels. Calatayud et al.^{3a} also present data for this cluster at the UHF/6-31G* and B3LYP/6-31G* levels. References 3a and d get different lowest energy structures at these theory levels. Pykavy et al.^{3d} calculate the structure of the lowest triplet state of V_2O_4 at the B3LYP and PB86/TZVP levels and find a stable cis-ring structure only. The energy difference between the cis-ring and trans-ring structures is small and calculational level dependent. Calatayud et al.^{3a} and Vyboishchikov et al.²¹ find both ring and linear structures for V_2O_5 , with the ring structures being more stable (20 kcal/mol) at the B3LYP/6-31G*, B3LYP, PB86/TZVP, DZP, and D(T)ZVP levels. Justes et al.^{3c} have calculated one of the structures for $V_4O_9^+$.

In the present study, we apply 118, 355, and 193 nm laser light to ionize neutral vanadium oxide clusters in the gas phase. The goal is to determine the neutral particle or “molecule” distribution present in the supersonic cluster beam. This characterized neutral distribution of vanadium oxide species can then be employed to study the reactions and properties of the generated species. Of the three ionization wavelengths chosen for this study, only 118 nm single photon ionization can ionize the vanadium oxide clusters without fragmentation. The averaged TOF mass peak widths observed with 118 nm ionization are the same as the seeded Nd:YAG pulse time width (~ 8 ns), and the individual ion peak widths are the same as the mass detector electron transit time (~ 1.7 ns). The observed V_mO_n mass spectra under these conditions are different for different O_2 contents (0.1–6%) in the expansion gas. Density functional theory calculations are employed to generate structures, energies, vibrations, and excited electronic states for a number of the observed clusters.

We also obtain spectra for the $\tilde{B}^2B_2 \leftarrow \tilde{X}^2A_1$ transition of vanadium dioxide (VO_2). The electronic transition can be detected at both the VO^+ and VO_2^+ mass channels. Rotational and vibrational temperatures can be determined for VO_2 along with values of ν_1 and ν_2 for both electronic states.

II. Experimental Procedures

The detailed experimental setup is given in earlier publications from this laboratory.^{16,19} Briefly, vanadium oxide clusters are generated in a supersonic expansion into a vacuum system by laser ablation of a metal foil into a flow of 0.1–6% O_2 in He at 100 psig. The 0.25 mm vanadium metal foil (99.7%) is purchased from Aldrich. Clusters grow under high pressure (probably ~ 10 psi) as the ablated metal plasma expands into the oxygen/helium mixture. The temperature at which they grow is probably near the initial plasma temperature (~ 3000 K).

The resulting clusters pass through an electric field region to remove ions created in the metal ablation/metal oxide growth process. Neutral vanadium oxide clusters pass through a 2 mm aperture skimmer into the ionization region of a time-of-flight mass spectrometer (Wiley-McLauren design- R. M. Jordan Co.) and are ionized by one of three pulsed lasers: 193 nm, ArF; 355 nm, third harmonic of a seeded Nd:YAG 1.064 μm laser; or 118 nm, ninth harmonic of the seeded Nd:YAG laser. The 118 nm light is generated from the third harmonic of the seeded Nd:YAG laser (~ 25 mJ/pulse, maximum energy), tripled in a Xe/Ar mixture at 1:10 relative concentration for 200–500 Torr of total pressure.¹⁹

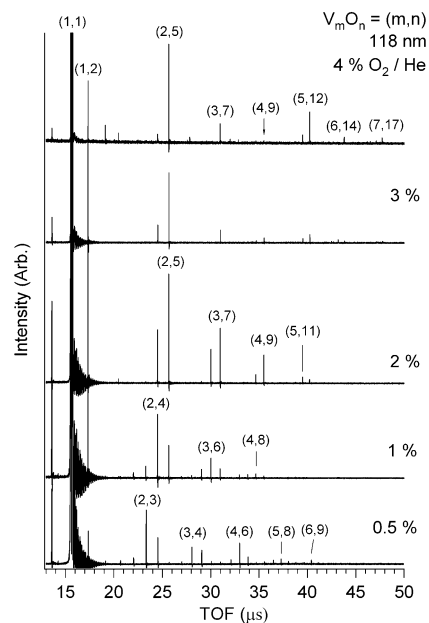


Figure 1. TOF mass spectra of vanadium oxide clusters ionized by 118 nm light as a function of different compositions of the O_2/He expansion gas mixture as indicated on each spectrum as a percentage of O_2 content in the He/O_2 mixture at 100 psig. The 118 nm light is generated by 25 mJ/pulse of 355 nm light focused in a 1:10 Xe/Ar mixture at 200 Torr of total pressure. The features at 19.1 and 20.5 μs are possibly due to $VO_3H_2^+$ and VO_4H^+ , respectively.

Synchronization of valve opening, laser pulsing, and detection is accomplished by a time delay generator. TOF mass spectroscopy signals are monitored by a Galileo microchannel plate (MCP) detector and acquired with a 500 MHz, 2 G sample/s Tektronix RTD 720 A transient digitizer connected to a personal computer. Each laser ionization pulse generates a full mass spectrum, which is individually stored and saved in the computer before the next pulse arrives. Averaged spectra are obtained at the end of each ~ 2000 pulse experimental run.

For electronic spectroscopy of neutral vanadium dioxide, a Nd:YAG pumped dye laser system is used for ionizing and fragmenting clusters. Details of the excitation/ionization schemes are presented in next section. The signal from the MCP detector is collected by a boxcar integrator and stored in a computer.

Optimized structures, isomers, ionization energies, relative conformation energies, and vibrational energies for the V_mO_n clusters are calculated at the BPW91/TZVP^{23,24} and BPW91/LANL2DZ-D95^{23,25} levels employing the Gaussian 98 program.²⁶ Structures are visualized with the MOLKEL program.²⁷

III. Results

1. Mass Spectra of Neutral Vanadium Oxide Clusters.

Figure 1 shows TOF mass spectra of V_mO_n clusters, observed through 118 nm ionization, for different compositions of the O_2/He expansion/reaction gas mixture (0.5–4.0% O_2 at 100 psig of total pressure). For these spectra, the mass peaks have an average width of ~ 8 ns, which corresponds to the time profile of the seeded Nd:YAG laser. This line width indicates that the neutral clusters are ionized without fragmentation,¹⁹ as will be discussed in section IV below. Higher concentrations of O_2 (to 6% O_2) in the expansion/reaction gas do not change the observed cluster distribution. For $< 3\%$ O_2 in the expansion reaction gas, the cluster distribution and species present change, and oxygen deficient vanadium oxide clusters begin to appear in the neutral cluster distribution. Under saturated O_2 growth conditions ($> 3\%$ O_2/He), stable clusters of the form $(VO_2)_x(V_2O_5)_y$ are found.

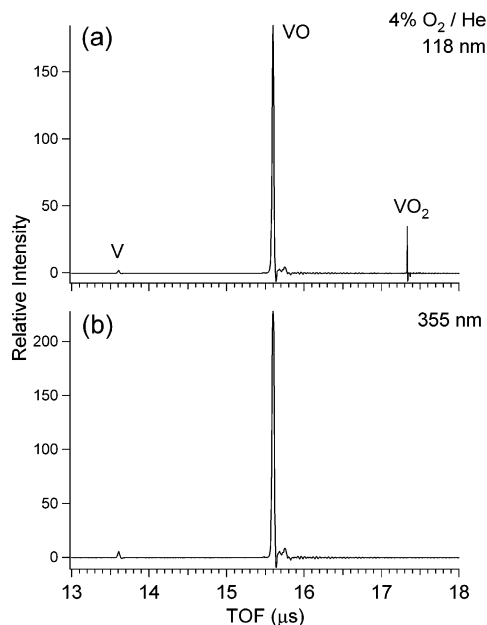


Figure 2. TOF mass spectra of vanadium oxide clusters in the region of VO_m ($m = 0-2$) observed by (a) 118 nm plus 355 nm ionization and (b) only 355 nm (25 mJ/pulse) ionization with 4% O_2/He expansion gas. The VO_2 is the most intense, purely single photon ionization feature in the mass spectra of V_mO_n neutral clusters.

At lower O_2 concentrations, the observed clusters are kinetically controlled by the growth process dynamics (e.g., diffusion, temperature, ...).

The neutral cluster distribution is not constant throughout the gas pulse, as can be readily observed in the detailed mass spectra. Larger clusters appear at the ionization region of the TOF mass spectrometer at later times in the pulse because (1) they take longer to grow in the reaction zone (plasma plus O_2) of the nozzle and (2) they are more difficult to accelerate to the He beam velocity ($\propto kT$) due to their increased inertia (“velocity slip”).^{19,28} These trends appear applicable even for kinetically controlled growth conditions (0.5% O_2/He mixtures); at early times in the expansion, V_3O_4 is most intense for the V_3O_x series, and at later times, V_3O_7 becomes more intense. For saturated O_2 growth conditions, these trends give way simply to the observation of larger clusters, in general, as found for the series V_2O_5 , V_3O_7 , V_4O_9 , V_5O_{12} , V_6O_{14} , and V_7O_{17} . Clusters V_8O_{19} and V_9O_{20} have also been observed.

Since 118 nm light is generated by tripling 355 nm light, residual 355 nm light (although defocused to ~ 8 mm) also appears at the ionization region of the TOF mass spectrometer and can thereby cause some neutral cluster ionization/fragmentation through multiphoton processes. Figure 2 presents this effect. Note that the broad VO feature is due almost entirely to 355 nm larger cluster ionization/fragmentation, while the sharp (~ 8 ns) VO_2 feature is due solely to 118 nm single photon ionization. Figure 3 presents mass spectra for larger clusters ionized by 118 and 355 nm light. Spectra a and b were obtained under the same conditions except that the 355 nm tripling cell was evacuated for spectrum b. This shows that spectrum a (except for VO^+) is due solely to 118 nm light ionization and that the line widths (8 ns) for the features with masses greater than VO^+ imply that no fragmentation has occurred in the ionization process (for the time range $\sim 1 \text{ ns} \leq t \leq 10 \mu\text{s}$).¹⁹ The V_2O_5 feature has been maximized by laser timing and TOF deflection plates. Fragmented species from 355 nm multiphoton ionization in spectra a and b are discriminated against, except for V^+ and VO^+ signals, by maximizing the 118 nm signal and

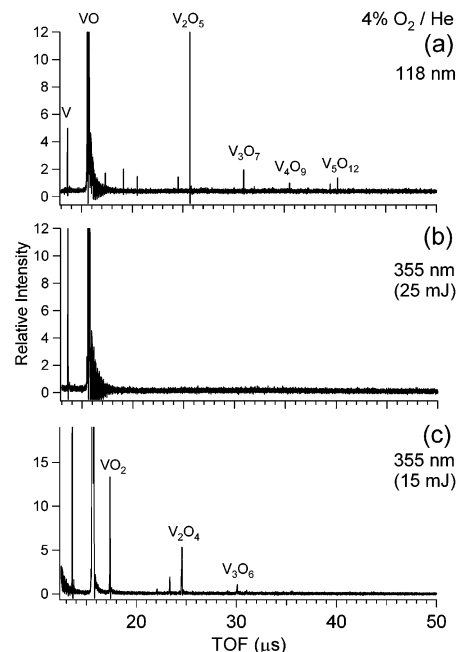


Figure 3. TOF mass spectra of vanadium oxide clusters with (a) 118 nm, (b) 355 nm (25 mJ/pulse), and (c) 355 nm (15 mJ/pulse) ionization. The 4% O_2/He expansion gas is used. Mass spectrum b is measured by evacuating the Xe–Ar gas cell. Spectrum b is measured under the same experimental conditions as those for spectrum a for which the 118 nm ionization signal has been optimized. Spectra c is measured by optimizing conditions for the 355 nm ionized cluster signal.

minimizing the 355 nm signal. The spectrum of Figure 3c is obtained by maximizing the timing for the detection of observed fragmented clusters seen in the spectrum. The features of spectrum c have line widths of ~ 90 ns. Note that the stable, most intense neutral clusters under O_2 saturated growth conditions as given in the figure are of the form $(\text{VO}_2)_x(\text{V}_2\text{O}_5)_y$.

The TOF mass spectra of neutral clusters ionized by 193 nm light are presented in Figure 4. These spectra are obtained under exactly the same experimental conditions as those in Figure 1 except for the ionization laser wavelength. The mass spectra of V_mO_n clusters reported in ref 16 correspond to spectra c, d, and e of Figure 4. As the O_2 concentration in the expansion gas changes from 0.5 to 3%, the clusters observed are more oxygen rich, as shown for V_2O_n , V_3O_n , V_4O_n , V_5O_n , and V_6O_n clusters. Nonetheless, the species observed with 118 nm ionization $[(\text{VO}_2)_x(\text{V}_2\text{O}_5)_y]$ under O_2 saturated growth conditions are not observed with 193 nm multiphoton ionization due to fragmentation of the neutral clusters in the ionization process while the 15 ns ArF excimer laser pulse is on. In all instances, the 193 nm detected clusters are more oxygen deficient (due to loss of oxygen atoms in the multiphoton ionization process) than those detected with 118 nm single photon ionization. Note, too, that the mass features in Figure 4 are much broader than those in Figure 1. Moreover, this line width difference increases for higher concentrations of O_2 in the expansion.

2. DFT Calculation for Neutral Vanadium Oxide Clusters.

As emphasized above, the 118 nm ionization TOF mass spectra of V_mO_n clusters reveal the true stable, neutral vanadium oxide cluster distributions for the given specific growth conditions appropriate for the chosen synthesis conditions of oxygen concentration, timing, backing pressure, and so forth. To obtain some insight into the structure, energetics, fragmentation, ionization energy, vibrations, and stability of these species, we have employed density functional theory (DFT) calculations at the highest levels available to us to address these cluster properties.

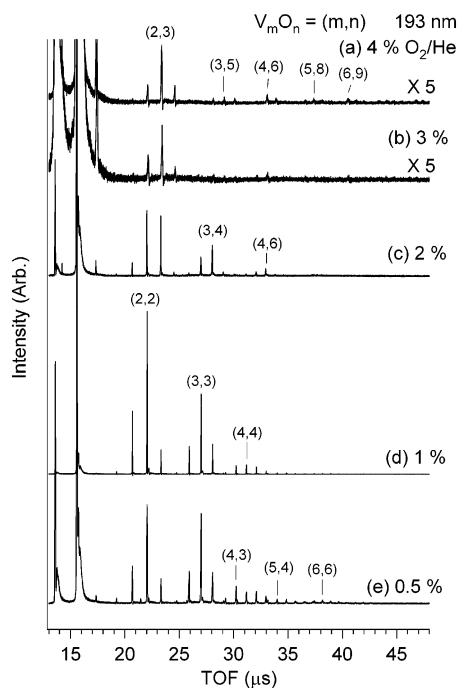


Figure 4. TOF mass spectra of vanadium oxide clusters as a function of O_2 concentration in the expansion gas observed by 193 nm laser ionization. Each spectrum is labeled to show the O_2 concentration in the expansion gas.

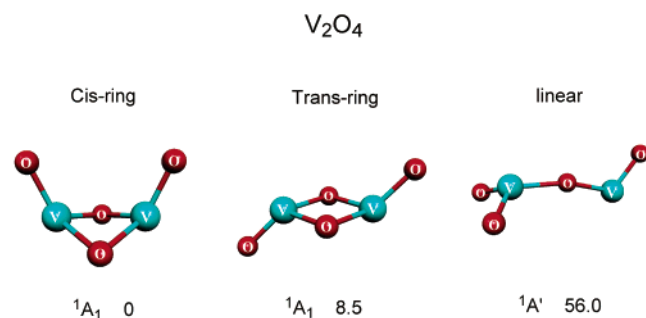


Figure 5. Optimized structures of V_2O_4 based on DFT calculations at the BPW91/TZVP level. The energy difference from the lowest energy cis structure is given in kilocalories per mole for the high energy isomers.

The present DFT calculations are performed at the BPW91/TZVP^{23,24} and PBW91/LANL2DZ/D95^{23,25} levels. The LANL2DZ/D95 basis sets²⁵ are respectively an effective core potential set for vanadium and a D95 set for oxygen. We are presently calculating the properties of all species observed for neutral V_mO_n clusters with $m \leq 5$ and studying their reactions with SO_2 , but in this report, we will only present data for the O_2 saturated growth, stable, neutral clusters V_2O_4 , V_2O_5 , V_3O_7 , and V_4O_9 .

Figure 5 presents optimized structures of the neutral cluster V_2O_4 at the BPW91/TZVP level. The energy difference between the cis- and trans-ring structures is small, and these two isomers can change relative energy positions depending on the applied calculational level (functional, basis set, etc.).^{3a,d} The present calculations show that the nonplanar (30°) cis-ring structure is more stable than the nearly planar trans-ring structure by roughly 8 kcal/mol. Almost surely, both structures are present under our experimental conditions. (VO_2 is determined to have a vibrational temperature of $700\text{ K} = 487\text{ cm}^{-1} = 1.4\text{ kcal/mol}$; $\sim 50\%$ of the V_2O_4 species could have the high energy isomer structure at this temperature.) The linear structure at ~ 60

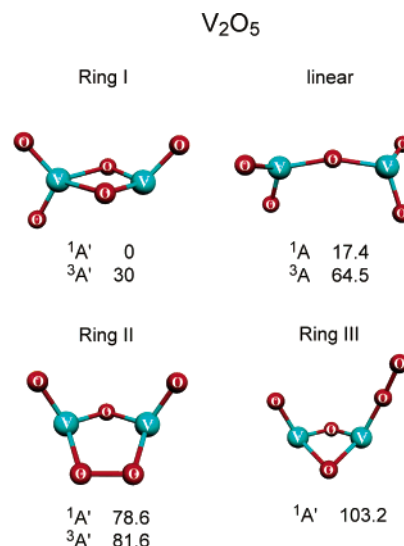


Figure 6. Optimized structures for V_2O_5 based on DFT calculations at the BPW91/TZVP level. The energy difference from the lowest energy structure ring I is given in kilocalories per mole for singlet and triplet electronic states of various isomers.

TABLE 1: Calculated Energy Differences (kcal/mol) for Structural Isomers of V_2O_5 in the Singlet Electronic Ground State

	ring I	linear	ring II	ring III
BPW91/TZVP	0	17.43	78.59	103.2
BPW91/LANL2DZ	0	12.25	76.12	

kcal/mol higher in energy is probably not present in the beam and will cool to one of the lower energy geometries if generated in the O_2 /metal plasma reaction in the ablation nozzle.

Optimized structures for the V_2O_5 neutral clusters are given in Figure 6. We have, as a test, calculated these structures at the BPW91/TZVP and BPW91/LANL2DZ/D95 levels, and the structure relative energies are presented in Table 1 for V_2O_5 . Figure 6 shows the relative energies of the structures for the $^1A'$ and $^3A'$ energy levels of V_2O_5 . Both the ring I and linear structures could be coexisting isomers for our experimental conditions, but most likely, the ring I structure is dominant for this ~ 15 kcal/mol energy difference between the two isomers. These calculations predict a $\tilde{a}^3A' \leftarrow \tilde{X}^1A'$ electronic transition for these structures at $10\,500\text{ cm}^{-1}$ (ring I) and $16\,485\text{ cm}^{-1}$ (linear). We are presently searching for these transitions.

Calculations for the structure and relative energies of neutral V_3O_7 species are presented in Figure 7 at the BPW91/TZVP level. Table 2 shows a comparison between the BPW91/TZVP and /LANL2DZ/D95 levels for this cluster isomer set for the two lowest energy isomers (I and II of Figure 7). The agreement between the TZVP and effective core potential basis set structures and energies seems quite reasonable. Note that for the V_3O_7 neutral cluster the lowest energy isomer has a three-dimensional (double ring) structure. Both structures I and II can be present in the beam. We expect that the higher energy isomers will probably relax to one of these two lower energy isomers in the cooling process.

Optimized structures and relative energies for the V_4O_9 neutral species are given in Figure 8. A number of these structures are now three-dimensional in nature. Isomer structures I, II, and III may well be present in the expansion, while the others are probably depopulated in the cooling process. DFT results for V_2O_5 and V_3O_7 suggest that the BPW91/LANL2DZ calculational level gives reliable high level results for structures and relative isomer energies.

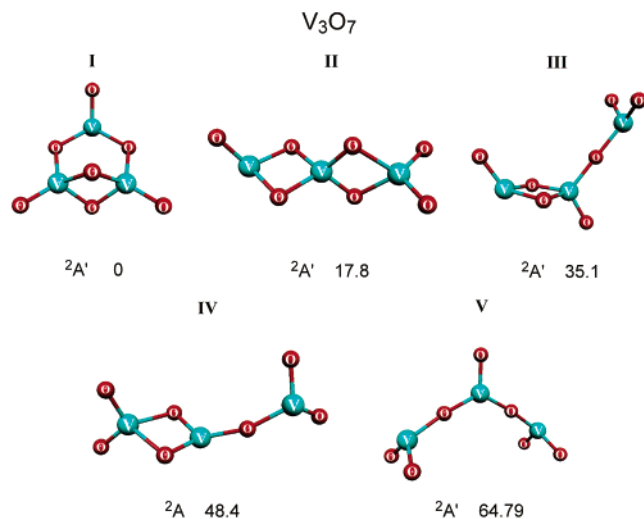


Figure 7. Optimized structures of V_3O_7 based on calculations at the BPW91/TZVP level. The energy difference from the lowest energy structure I is given in kilocalories per mole for the higher energy isomers.

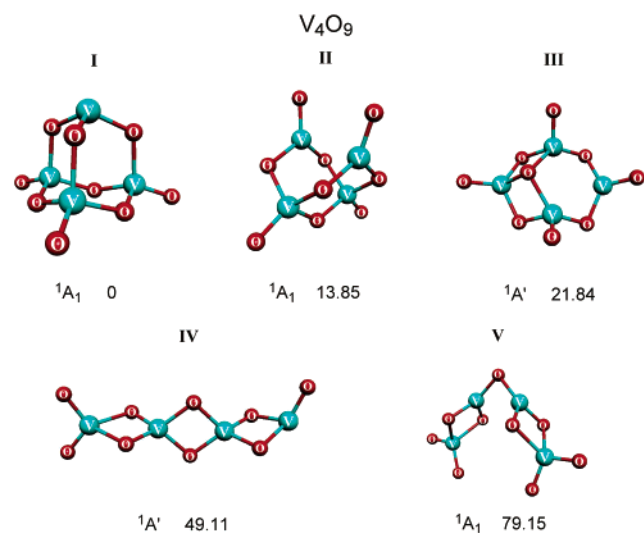


Figure 8. Optimized structures of V_4O_9 based on calculations at the BPW91/LANL2DZ level. The energy difference from the lowest energy structure I is given in kilocalories per mole for the higher energy isomers.

TABLE 2: Calculated Energy Differences (kcal/mol) for Structural Isomers of V_3O_7 in the Doublet Electronic Ground State

	I	II	III	IV	V
BPW91/TZVP	0	17.81	35.09	48.39	64.79
BPW91/LANL2DZ	0	19.80			

TABLE 3: Calculated Ionization Energy (eV) of Vanadium Oxide Clusters at BPW91/LANL2DZ (TZVP)

	VO	VO ₂	VO ₃	VO ₄	V ₂ O ₃	V ₂ O ₄ ring	V ₂ O ₅ ring	V ₂ O ₅ linear	V ₂ O ₆
vertical	7.55 (7.33)	8.97 (8.47)	11.64 (11.38)				10.58	10.25	10.81
adiabatic	7.52 (7.29)	8.83 (8.32)	11.51 (11.25)	11.24	6.64	8.46	10.26		10.53

Vertical and adiabatic ionization energies for clusters VO, VO₂, VO₃, VO₄, V₂O₃, V₂O₄, V₂O₅, and V₂O₆ are calculated and presented in Table 3. These values ± 0.5 eV serve as a rough guide for an estimate of which species should be stable upon 10.5 eV ionization and also which species should be

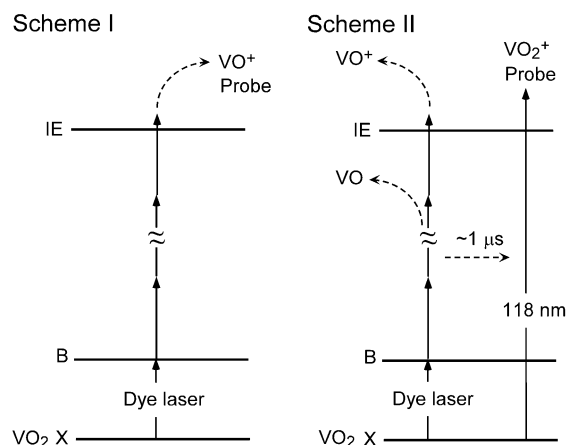


Figure 9. Excitation/ionization scheme for MPI spectroscopy (Scheme 1) for the VO⁺ channel and mass selective ion dip spectroscopy (Scheme 2) of the 118 nm ionization signal for the VO₂⁺ channel. In both schemes, the electronic transition is observed by scanning the dye laser. In Scheme 2, the scanning dye laser is introduced before the probe (118 nm) laser.

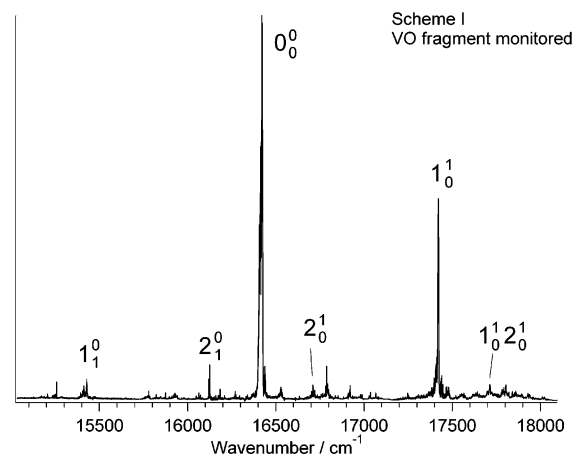


Figure 10. Electronic spectrum observed at the VO⁺ mass channel by scanning the excitation laser. The assignment of observed transitions is mentioned in text and in Table 4.

possible to ionize with 10.5 eV ionization. Highly oxidized VO₃ and VO₄ may not be accessible for ionization under our experimental conditions by a single photon process. Note that the TZVP basis set values of ionization energies are ~ 0.3 eV lower than those for the LANL2DZ basis set.

3. Electronic Spectroscopy for VO₂($\tilde{B}^2B_2 \leftarrow \tilde{X}^2A_1$). The two detection techniques for observing the mass resolved excitation spectrum of a given cluster are presented in Figure 9. One can observe the changes in the mass spectral peak intensity for a fragment of the cluster created as the parent cluster absorbs energy from a tunable laser (Scheme 1 of Figure 9), or one can observe a change in the parent mass feature intensity itself created by fragmentation due to tunable laser light absorption (Scheme 2 of Figure 9). The spectrum of the $\tilde{B} \leftarrow \tilde{X}$ transition of VO₂ can be detected by both methods. Figure 10 presents the overall spectrum for the VO₂ transition detected at the VO⁺ mass channel, as measured by Scheme 1 in Figure 9. VO⁺ signal changes are obtained by scanning the dye laser wavelength. If the dye laser wavelength is resonant with an electronic transition of a cluster, a VO⁺ photofragmented ion is generated and is observed as the enhanced signal of VO⁺. One cannot easily assign, however, to which cluster this observed electronic transition belongs due to the coexistence of various clusters in the cluster beam.

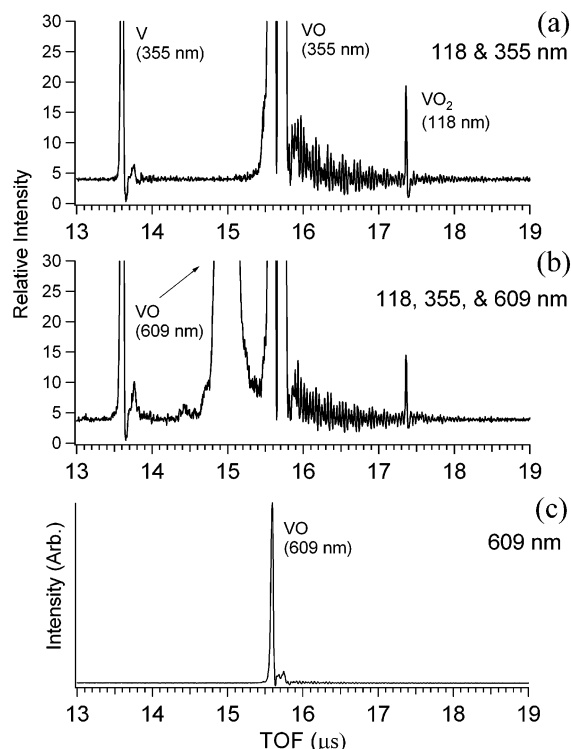


Figure 11. TOF mass spectra in the VO_x mass region obtained by ionization at (a) 118 and 355 nm, (b) 118, 355, and 609 nm, and (c) 609 nm ionization. Mass spectra a and b are acquired by detection timing with the 355 nm laser, and spectrum c is obtained by detection timing with the 609 nm dye laser. The 609 nm laser is introduced 7 μs earlier than the 118 and 355 nm lasers for spectrum b.

Scheme 2 in Figure 9 illustrates the excitation scheme for mass selective spectroscopy based on 118 nm single photon ionization. As described above, 118 nm single photon ionization does not cause cluster fragmentation for metal oxide clusters. If a wavelength resonant with an electronic transition of the probed cluster causes cluster fragmentation more efficiently than a nonresonant one, a mass selective electronic spectrum for the cluster is observed as a decrease of the probed 118 nm single photon ionization signal. If clusters fragment into the monitored mass channel, the fragmentation component would appear as an enhancement of the signal probed. The scanned (spectroscopy) laser must be introduced at the same time as, or earlier than, the 118 nm ionization (probe) laser.

Figure 11 shows the TOF mass spectra observed by (a) 118 and 355 nm, (b) 118, 355, and 608.969 nm ($16\,421.2\text{ cm}^{-1}$), and (c) 608.969 nm ionization in the VO_x mass region. Spectra b and c are observed by Schemes 2 and 1 in Figure 9, respectively. In spectrum b, the 608.969 nm wavelength is the observed resonant energy of an electronic transition shown in Figure 9 (0_0^0). As seen in spectrum 11b, the 608.969 nm laser causes two changes in the mass spectrum: the appearance of a new VO^+ signal, which is generated by the 608.969 nm laser at $\sim 0.7\ \mu\text{s}$ earlier than the 355 nm VO^+ generated signal, and a decrease of the signal intensity of the VO_2^+ signal ionized by the 118 nm laser. Figure 11c shows the mass spectrum observed by 608.969 nm resonant multiphoton ionization alone. The 608.969 nm laser creates only a VO^+ signal. For this experiment, the energy/pulse ($\sim 3\text{ mJ}$) of the 608.969 nm laser is adjusted so that the VO^+ signal is detected only for the wavelength resonant with the electronic transition. With high pulse energy (10 mJ) of the dye laser at $\sim 609\text{ nm}$, larger clusters with nonresonant multiphoton ionization/fragmentation are observed.

Parts a and d of Figure 12 show dip spectra of the VO_2^+ signal detected by 118 nm ionization, parts b and e show multiphoton ionization (MPI) spectra detected for VO^+ , and parts c and f show simulated spectra for VO_2 . Figure 12a–c presents spectra of the transition origin (0_0^0), and Figure 12d–f presents spectra of the ν_1 vibronic transition. Rotational envelope simulation for these transitions is performed with rotational constants obtained at the BPW91/TZVP level DFT calculation for the electronic ground state of neutral VO_2 and VO_2^+ singlet cation: for this approximation, we assume that the geometrical structure of the cation is similar to the excited state structure. Note that the rotational envelopes for the two detection methods (Schemes 1 and 2 of Figure 9) are slightly different. We attribute this difference to the, in principle, separate paths the VO^+ fragment generation and the VO_2^+ parent take to ionization. The VO_2^+ detected envelope relies mostly on the $\tilde{\text{B}} \leftarrow \tilde{\text{X}}$ and $\text{I} \leftarrow \tilde{\text{X}}$ transitions (Scheme 2), while the VO^+ detected envelope depends, in principle, on the multiple transitions for $\text{VO}_2 \rightarrow \text{VO}^+$ (Scheme 1). Neither is exactly like the simulation (Figure 12f) because of the simulation assumptions and approximations.

The best fit is for a rotational temperature (T_{rot}) of $\sim 50 (\pm 5)$ K. The dip spectra of VO_2^+ are observed by Scheme 2 in Figure 11. The MPI spectra for VO^+ in Figure 12 are expanded spectra of Figure 10 observed by Scheme 1. The dip spectra of VO_2^+ correspond to MPI spectra for VO^+ . Laser light at the observed resonant wavelength decreases the population of VO_2 by resonant multiphoton ionization/fragmentation. Therefore, the observed transitions are assigned to originate with the VO_2 cluster. Table 4 gives the observed vibronic transitions for VO_2 and their assignments. The details of the assignments are discussed in the next section.

The intensity ratio for the 1_1^0 and 1_0^1 transitions yields a vibrational temperature (T_{vib}) of $\sim 700 (\pm 50)$ K. This vibrational temperature is similar to that found for VO .¹⁶ A vibrational temperature could also be extracted for the $2_1^0/2_0^1$ intensity ratio, but the 2_0^1 transition seems to be perturbed and perhaps its intensity is shared between the features at $16\,710.8$ and $16\,788.7\text{ cm}^{-1}$ (see Table 4).

IV. Discussion

1. Neutral Cluster Distribution. The width of a mass feature in a TOF mass spectrum can reveal information on the nature of the ion (daughter vs parent) detected. If the cluster does not fragment during the ionization process (parent ion generated), the detected species represents a member of the neutral cluster distribution prior to ionization. The contributions to the ion peak's width include the following:¹⁹ (1) the laser focus size, (2) the laser time width, (3) the m/z value of the mass feature, (4) the MCP electron transit time ($\sim 1.7\text{ ns}$), and (5) the fragmentation time. The contribution to the mass spectral peak width due to spatial distribution of the ionization process increases with increasing mass. The 118 nm ionization is by a single photon (10.5 eV, $\sim 10^{11}$ photons/pulse, $< 100\ \mu\text{m}$ focus), and the spatial distribution of the laser in the TOF ionization region does not contribute significantly to the peak line width for $m/z < 500$. Thus, the averaged line width (~ 2000 laser pulses) is found to be the seeded Nd:YAG laser time width, $\sim 8.0\text{ ns}$.

Fragmentation during the ionization process within the time range $1\text{ ns} \leq \Delta t \leq 10\ \mu\text{s}$ will affect the observed line width of TOF mass features due to the increased spatial distribution of the ions created and any additional velocity the species might acquire in the fragmentation process. These observations are not restricted to the vanadium oxide system but are consistent

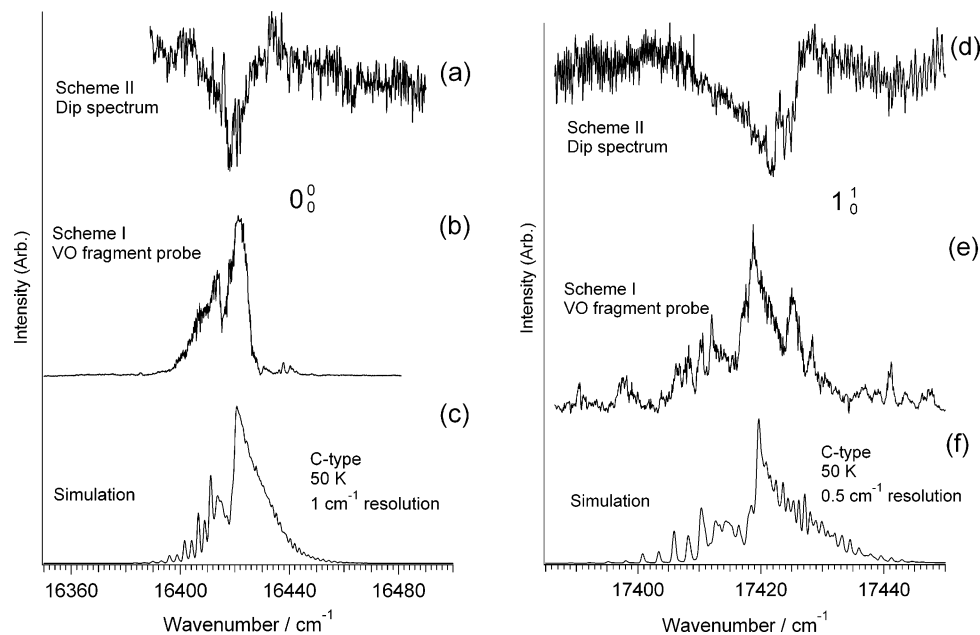


Figure 12. 0_0^0 transition (a, b, and c) and 1_0^1 transition (d, e, and f) for the $\text{VO}_2^+ \tilde{B} \leftarrow \tilde{X}$ spectrum: parts a and d show ion dip spectra at the VO_2^+ mass channel detected by Scheme 2 and parts b and e show MPI spectra at the VO^+ mass channel detected by Scheme 1. Parts c and f show rotational simulations for the 0_0^0 and 1_0^1 transitions, respectively. Rotational constants of 2A_1 neutral VO_2 and 1A_1 VO_2^+ obtained at the BPW91/TZVP level are used as simulation parameters for the 2A_1 and 2B_2 states, respectively. Simulation of c-type transitions at $T_{\text{rot}} \sim 50$ K reproduces the observed spectra. See the text for a more detailed discussion of the rotational envelopes for the observed and calculated transitions.

TABLE 4: Observed Peak Positions (cm^{-1} , Vacuum) for the VO^+ Channel in the Region of the $\tilde{B}^2B_2 \leftarrow \tilde{X}^2A_1$ Transition of VO_2 and Assignments for the $\tilde{B}^2B_2 \leftarrow \tilde{X}^2A_1$ Transition of VO_2

observed for VO^+	assignment	photoelectron ^b
15 257.5		
15 428.2 ^a		
15 779.9	1_0^0	
15 823.2		
15 875.8		
15 928.0		
16 063.3		
16 119.0		
16 125.2 ^a	2_2^1	
16 270.2	2_1^0	
16 339.1	?	
16 421.2 ^a	0_0^0	$16\,410 \pm 800$
16 527.6		
16 710.8 ^a	2_0^1	
16 788.7 ^a	? ^c	
16 921.9		
17 421.7 ^a	1_0^1	
17 712.6	$1_0^1 2_0^1$	
17 804.7	$1_0^1 ?^c$	

^a Peaks are ascertained to belong to VO_2 by ion dip spectroscopy, as shown in Figure 10. ^bReference 11b. ^cThe observed peak belongs to VO_2 . It is not assigned, though it might be a ν_2 vibronic component.

with those made for Zr, Cu, Fe, and Ti oxides.¹⁹ Thus, the mass spectral peak line width serves as a good indication of the presence or absence of fragmentation in the neutral cluster ionization process.

Using 10.5 eV, single photon ionization for neutral V_mO_n clusters, all clusters, with the possible exception of VO_3 and VO_4 (calculated ionization energy ~ 11.5 eV, see Table 3), will be ionized. Most V_mO_n neutral clusters have an ionization energy in the range 7–10.5 eV.^{19,20} Thus, the cluster excess energy following ionization is ~ 0 –4 eV. This is not enough energy to break a V–O bond in such a cluster.^{4b} Even 5–6 eV of excess energy in such clusters would not yield fragmentation times

(RRKM estimates) within the appropriate time range for observable line width effect in large clusters ($m, n > 5$). Multiphoton, 355 and 193 nm ionization can of course cause fragmentation within this time range because many photons can be absorbed in the ionization process.^{15,18} Two photon ionization by 355 nm (3.5 eV) plus 118 nm photons for clusters with ionization energies larger than 10.5 eV is possible and should also not cause fragmentation of clusters.

With 118 nm ionization and for saturated oxygen growth conditions ($\geq 3\%$ O_2 in the He expansion gas), the observed clusters have the form $(\text{VO}_2)_x(\text{V}_2\text{O}_5)_y$: VO_2 and V_2O_5 are the most intense features detected. These observations, coupled with the DFT calculated structures presented in Figures 5–8, suggest a growth mechanism for V_mO_n neutral clusters. V_2O_4 clusters (Figure 5) can clearly arise from the bonding of two VO_2 (C_{2v}) clusters. V_2O_5 has two structures, ring I and linear (see Figure 6), that probably coexist in the neutral beam. Both seem to be accessible through the binding of VO_2 and VO_3 . The most stable V_3O_7 structures (I and II of Figure 7) can be formed from the two low energy V_2O_5 structures (Figure 6) by the addition of VO_2 clusters without a large displacement of the atoms. In a like manner, V_4O_9 (Figure 8) structures I, II, and III can be generated from structure I of V_3O_7 plus VO_2 with only one V–O bond cleavage. V_4O_9 structures I, II, and III can also be formed from linear V_2O_5 (Figure 6, II) and two VO_2 species without bond cleavage. These syntheses probably take place in the ablation plasma/ O_2 gas mixing region of the nozzle at temperatures possibly as high as 3000–5000 K.

2. Multiphoton Cluster Fragmentation. From a comparison of Figures 1, 3, and 4, one notes that more oxygen poor cluster ions are observed by 193 and 355 nm ionization than by 118 nm ionization. The line widths of the observed mass peaks for 193 and 355 nm ionization are broader (up to a factor of 10) than those observed for 118 nm ionization especially at higher oxygen concentrations in the expansion/reaction gas. This means that fragmentation has occurred within 1 ns to 10 μs following the ionization laser pulse. On the basis of the calculations

TABLE 5: Vibrational Energies (cm⁻¹) for the \tilde{B}^2B_2 and \tilde{X}^2A_1 States of VO₂

	this study	photoelectron ^a	matrix isolation ^b	BPW91/TZVP	BPW91/LANL2DZ
			\tilde{X}^2A_1		
ν_1	993.0	970 ± 40	946.3	1003.1	998.1
ν_2	296.0			338.7	319.6
ν_3			935.9	985.0	996.2
			\tilde{B}^2B_2		
ν_1	1000.5				
ν_2	289.6				

^a Reference 11. ^b Reference 29.

presented in Figures 5–8 and the energies for single V–O bonds in these clusters, one can suggest that cluster multiphoton fragmentation occurs through the loss of oxygen atoms and not V_mO_n units, for laser intensities <10⁹ W/cm² (1 mJ/10 ns pulse, focused to ~0.1 mm diameter spot).

References 16 and 18 apply a covariance mapping analysis to learn about cluster growth and fragmentation pathways for different metal oxides, including vanadium oxide, employing 193 nm ionization. They correctly concluded that, for the vanadium oxide system, the cluster ions observed by 193 nm ionization are related by a growth process. They further suggested, therefore, that these ions represented the neutral cluster V_mO_n distribution because no true parent ions remain in the mass spectrum. In the absence of fragmentation, employing 118 nm ionization, the neutral cluster distribution can be identified. Covariance mapping distinguishes growth and fragmentation relations between cluster species, but if only one or the other pathway is represented by the observed mass features, distinction between the two pathways can be difficult.

3. Electronic Transition of VO₂. The observed transitions shown in Table 4 and Figure 10 are assigned to VO₂, as mentioned in the previous section. Wu et al.^{11b} report photoelectron spectra of VO₂ consisting of an unresolved broad feature at ~16 410 cm⁻¹. They assign this feature to the \tilde{B} state of VO₂. Our observed transitions correspond to the energy of the B state feature of their photoelectron spectrum of VO₂⁻. Knight et al.^{21b} report an ab initio calculation of VO₂ in conjunction with an ESR study. According to their multireference singles and doubles configuration interaction (MRSDCI) calculation with ROHF orbitals, the electronic excited states ²A₂ and ²B₂ have a higher energy by ~2.0 and ~3.0 eV, respectively, than the electronic ground state ²A₁.

As shown in Figure 12, rotational simulation of a c-type transition reproduces the observed features 0₀⁰ and 1₀¹. Additionally, all the intense transitions for VO₂ listed in Table 4 (marked with “a”) that can be observed to decrease the 118 nm generated VO₂⁺ signal within the Scheme 2 detection method of Figure 9 also have the c-type rotational structure of VO₂. VO₂ has the C_{2v} structure and the three normal modes ν_1 (symmetric stretch), ν_2 (bend), and ν_3 (antisymmetric stretch), which belong to a₁, a₁, and b₁ symmetry, respectively. The c-type rovibronic structure means that the observed vibronic features belong to symmetry B₂. Therefore, we can expect that the electronic excited state has A₂ or B₂ symmetry.

If the electronic transition is $\tilde{B}^2A_2 \leftarrow \tilde{X}^2A_1$, one can expect to observe vibronic transitions involving ν_3 only ($\Delta v = \pm 1, \pm 3, \dots$); however, the observed spectrum has the structure of an allowed 0₀⁰ transition plus ν_1, ν_2 vibronic hot and cold bands. These all belong to an electronic transition of VO₂ and all have c-type rotational contours. Therefore, we assign the observed electronic transition of VO₂ to $\tilde{B}^2B_2 \leftarrow \tilde{X}^2A_1$, assigned as shown in Table 4.

Table 5 summarizes the vibrational energies for VO₂ in the \tilde{B}^2B_2 and \tilde{X}^2A_1 states. ν_3 vibrational energy is not obtained experimentally due to low or zero intensity for the b₁ modes for a C_{2v} molecule in the $\tilde{B}^2B_2 \leftarrow \tilde{X}^2A_1$ transition.

The observed transition is assigned to VO₂ because the ion dip spectrum (Scheme 2 of Figure 9) is observed on the 118 nm ion signal for VO₂. This spectroscopic technique also proves that neutral VO₂ is ionized to VO₂⁺ by 118 nm single photon ionization without fragmentation.

V. Conclusions

In this study, single photon, 10.5 eV ionization has been employed to determine the distribution of neutral vanadium oxide clusters generated in the gas phase by laser ablation of the metal into mixtures of oxygen and helium. DFT calculations of neutral cluster structures and ionization energies suggest that the observed cluster ions generated, employing 10.5 eV ionization, are indeed representative of the neutral cluster distribution prior to ionization. Of the clusters calculated, only VO₃ and VO₄ have higher ionization energies (11.5 eV); the VO₃ cluster is observed only for conditions such that 355 plus 118 nm two photon ionization is possible. These conclusions are supported by RRKM calculations, line width data, and available ionization energy data. Neutral clusters for saturated oxygen growth conditions are found to be of the form (VO₂)_x(V₂O₅)_y. Cluster growth prior to ionization is suggested to be through VO₂ or V₂O₅ addition to (VO₂)_a and (V₂O₅)_b species, such that the stable neutrals (saturated oxygen growth) are VO₂, V₂O₄, V₂O₅, V₃O₇, V₄O₉, V₅O₁₂, V₆O₁₄, V₇O₁₇,

Cluster fragmentation due to multiphoton absorption during the ionization processes associated with relatively low laser energy/pulse 193 and 355 nm ionization is suggested to occur by the loss of oxygen atoms singly bonded to vanadium atoms in the cluster, based on DFT structure calculations and energetic considerations.

Observation of the $\tilde{B}^2B_2 \leftarrow \tilde{X}^2A_1$ transition for VO₂ at 16 421.2 cm⁻¹ (0₀⁰) yields rotational and vibrational temperature information for small clusters: $T_{\text{rot}} \sim 50$ K and $T_{\text{vib}} \sim 700$ K. This spectrum is uniquely assigned to the VO₂ cluster through ion dip spectroscopy, employing 118 nm single photon ionization for the clusters. These results further support the contention that 118 nm radiation at ~1 μJ/pulse energy does not fragment the clusters.

Acknowledgment. These studies are supported in part by the US DOE, Phillip Morris USA, and the National Science Foundation.

References and Notes

- (1) (a) Mutttert, E. L.; Rodin, T. N.; Brand, R. *Chem. Rev.* **1979**, *79*, 91. (b) Mutttert, E. L.; Wexler, R. M. *Surv. Prog. Chem.* **1983**, *10*, 61.
- (2) (a) Braunstein, P.; Oro, L. A.; Raithby, P. R. *Metal Clusters in Chemistry*; Wiley-VCH: Weinheim, Germany, and New York, 1999; Vols. 1–3. (b) Hackett, P. A.; Mitchell, S. A.; Rayner D. M.; Simard B. *Metal-Ligand Interactions*; Kluwer: Amsterdam, The Netherlands, 1996; p 289. (c) Smalley R. E. *Metal-metal bonds and clusters in chemistry and catalysis*; Texas A&M University: College Station, TX, 1989; p 249.
- (3) (a) Calatayud, M.; Andres, J.; Beltran, A. *J. Phys. Chem. A* **2001**, *105*, 9760. (b) Wu, X.; Ray, A. K. *J. Chem. Phys.* **1999**, *110*, 2437. (c) Phkavy, M.; van Wüllen, C. *J. Phys. Chem. A* **2003**, *107*, 5566. (d) Pykavy, M.; van Wüllen, C.; Sauer J. *J. Chem. Phys.* **2004**, *120*, 4207. (e) Justes, A. R.; Mitric, R.; Moore, N. A.; Bonacic-Koutecky, V.; Castleman, A. W., Jr. *J. Am. Chem. Soc.* **2003**, *125*, 6289.
- (4) (a) Liyanage, R.; Conceicao, J.; Armentrout, P. B. *J. Chem. Phys.* **2002**, *116*, 936. (b) Xu, J.; Rodgers, M. T.; Griffin, J. B.; Armentrout, P. B. *J. Chem. Phys.* **1998**, *108*, 9339. (c) Sievers, M. R.; Armentrout, P. B.

- J. Chem. Phys.* **1995**, *102*, 754. (d) Su, B.-X.; Hales, D. A.; Armentrout, P. B. *J. Chem. Phys.* **1993**, *99*, 6613.
- (5) (a) Zemski, K. A.; Justes, D. R.; Castleman, A. W., Jr. *J. Phys. Chem. B* **2002**, *106*, 6136. (b) Bell, R. C.; Zemski, K. A.; Justes, D. R.; Castleman, A. W., Jr. *J. Chem. Phys.* **2001**, *114*, 798. (c) Kooi, S. E.; Castleman, A. W., Jr. *J. Phys. Chem. A* **1999**, *103*, 5671. (d) Bell, R. C.; Zemski, K. A.; Castleman, A. W., Jr. *J. Phys. Chem. A* **1998**, *102*, 8293. (e) Bell, R. C.; Zemski, K. A.; Castleman, A. W., Jr. *J. Phys. Chem. A* **1999**, *103*, 1585. (f) Bell, R. C.; Zemski, K. A.; Kerns, K. P.; Deng, H. T.; Castleman, A. W., Jr. *J. Phys. Chem. A* **1998**, *102*, 1733.
- (6) Engeser, M.; Weiske, T.; Schroder, D.; Schwarz, H. *J. Phys. Chem. A* **2003**, *107*, 2855.
- (7) Yang, C. S.; James, A. M.; Rayner, D. M.; Hackett P. A. *J. Chem. Phys.* **1995**, *102*, 3129.
- (8) Pramann, A.; Koyasu, K.; Nakajima, A.; Kaya, K. *J. Chem. Phys.* **2002**, *116*, 6521.
- (9) Green, S. M. E.; Alex, S.; Fleischer, N. L.; Millan, E. L.; Marcy, T. P.; Leopold, D. G. *J. Chem. Phys.* **2001**, *114*, 2653.
- (10) Feigerie, B. S.; Corderman, R. R.; Bebashev, S. V.; Lineberger, W. C. *J. Chem. Phys.* **1981**, *74*, 1580.
- (11) (a) Zhai, H.-J.; Wang, L.-S. *J. Chem. Phys.* **2002**, *117*, 7882. (b) Wu, H.; Wang, L.-S. *J. Chem. Phys.* **1998**, *108*, 5310.
- (12) Minemoto, S.; Terasaki, A.; Kondow, T. *J. Electron Spectrosc. Relat. Phenom.* **2000**, *106*, 171.
- (13) Asmis, K. R.; Meijer, G.; Brümmer, M.; Kaposta, C.; Santambrogio, G.; Wöste, L.; Sauer, J. *J. Chem. Phys.* **2004**, *120*, 6461.
- (14) (a) Harrington J.; Weisshaar, J. C. *J. Chem. Phys.* **1992**, *97*, 2809. (b) O'Brien, T. A.; Albert, K.; Zerner, M. C. *J. Chem. Phys.* **2000**, *112*, 3192. (c) Spain, B. M.; Behm, J. M.; Morse, M. D. *J. Chem. Phys.* **1992**, *96*, 2511. (d) James, A. M.; Kowalczyk, P.; Langlois, E.; Campbell, M. D.; Ogawa, A.; Simard, B. *J. Chem. Phys.* **1994**, *101*, 4485.
- (15) Nieman, G. C.; Parks, E. K.; Richtsmeier, S. C.; Liu, K.; Pobo, L. G.; Riley, S. J. *High Temp. Sci.* **1986**, *22*, 115.
- (16) Foltin, M.; Stueber, G. J.; Bernstein, E. R. *J. Chem. Phys.* **1999**, *111*, 9577.
- (17) Fielicke, A.; Mitrić, R.; Meijer, G.; Bonažić-Koutecký, V.; von Helden, G. *J. Am. Chem. Soc.* **2003**, *125*, 15716.
- (18) Foltin, M.; Stueber, G. J.; Bernstein, E. R. *J. Chem. Phys.* **2001**, *114*, 8971.
- (19) (a) Matsuda, Y.; Shin, D. N.; Bernstein, E. R. *J. Chem. Phys.* **2004**, *120*, 4142. (b) Shin, D. N.; Matsuda, Y.; Bernstein, E. R. *J. Chem. Phys.* **2004**, *120*, 4150. (c) Shin, D. N.; Matsuda, Y.; Bernstein, E. R. *J. Chem. Phys.* **2004**, *120*, 4157. (d) Matsuda, Y.; Shin, D. N.; Bernstein, E. R. *J. Chem. Phys.* **2004**, *120*, 4165. (e) Matsuda, Y.; Bernstein, E. R. *J. Phys. Chem. A* **2005**, *109*, 314. (f) Bernstein, E. R.; Matsuda, Y. *Environmental Catalysis*; Marcel Dekker: New York, 2005.
- (20) (a) <http://webbook.nist.gov/chemistry>. (b) Albaret, T.; Finocchi, F.; Noguera, C. *J. Chem. Phys.* **2000**, *113*, 2238. (c) Persson, J. L.; Andersson, M.; Holmgren, L.; Åklint, T.; Rosén, A. *Chem. Phys. Lett.* **1997**, *271*, 61. (d) Boutou, V.; Lebeault, M. A.; Allouche, A. R.; Paulig, F.; Viallon, J.; Bordas, C.; Chevaleyre, J. *J. Chem. Phys.* **2000**, *112*, 6228. (e) Dai, B.; Tian, L.; Yang, J. *J. Chem. Phys.* **2004**, *120*, 2746.
- (21) (a) Vyboishchikov, S. F.; Sauer, J. *J. Phys. Chem. A* **2001**, *105*, 8588. (b) Knight, L. B., Jr.; Babb, R.; Ray, M.; Banisaukas, T. J., III; Russon, L.; Dailey, R. S.; Davidson, E. R. *J. Chem. Phys.* **1996**, *105*, 10237.
- (22) (a) Anstrom, M.; Topsoe, N.-Yu.; Dumesic, J. A. *J. Catal.* **2003**, *213*, 115. (b) Gilardoni, A.; Bell, A. T.; Chakraborty, A.; Boulet P. *J. Phys. Chem. B* **2000**, *104*, 12250. (c) Yin, X.; Fahmi, A.; Endou, A.; Miura, R.; Gunji, I.; Yamuchi, R.; Kubo, M.; Chatterjee, A.; Miyamoto, A. *Appl. Surf. Sci.* **1998**, *130*, 539. (d) Czekaj, I.; Hermann, K.; Witko, M. *Surf. Sci.* **2003**, *545*, 85. (e) Witko, M.; Tokarz, R.; Haber, J. *Appl. Catal., A* **1997**, *157*, 23. (f) Robert, V.; Borshch, S. A.; Bigot, B. *Chem. Phys.* **1996**, *210*, 401. (g) Gubanov, V. A. *Chem. Phys.* **1975**, *11*, 319.
- (23) (a) Burke, K.; Perdew, J. P.; Yang, Y. *Electronic Density Functional Theory: Recent Progress and New Directions*; Plenum: New York, 1998. (b) Perdew, J. P. *Electronic Structure of Solids*; Akademie Verlag: Berlin, 1991; p 11. (c) Perdew, J. P.; Chevary, J. A.; Vosko, S. H.; Jackson, K. A.; Pederson, M. R.; Singh, D. J.; Fiol Hais, C. *Phys. Rev. B* **1992**, *46*, 6671; **1993**, *48*, 4978. (d) Perdew, J. P.; Burke, K.; Wang, Y. *Phys. Rev. B* **1996**, *54*, 16533. (e) Becke, A. D. *J. Chem. Phys.* **1996**, *104*, 1040.
- (24) (a) Schäfer, A.; Huber, C.; Ahlriches, R. *J. Chem. Phys.* **1994**, *100*, 5829. (b) Wachters, A. J. H. *J. Chem. Phys.* **1970**, *52*, 1033.
- (25) Hay, P. J.; Wadt, W. R. *J. Chem. Phys.* **1985**, *82*, 270, 284, 299.
- (26) Frisch, M. J.; Trucks, G. W.; Schlegel H. B.; et al. *GAUSSIAN 98*, revision A. 6; Gaussian, Inc.: Pittsburgh, PA, 1998.
- (27) Flukiger, P.; Luthi, H. P.; Portmann, S.; Weber, J. *Molekel 4.0*; Swiss Center for Scientific Computing: Manno, Switzerland, 2000.
- (28) (a) Shang, Q. Y.; Moreno, P. O.; Li, S.; Bernstein, E. R. *J. Chem. Phys.* **1993**, *98*, 1876. (b) Li, S.; Bernstein, E. R. *J. Chem. Phys.* **1992**, *97*, 792. (c) Im, H.-S.; Bernstein, E. R. *J. Chem. Phys.* **2000**, *113*, 7911.
- (29) Chertihin, G. V.; Bare, W. D.; Andrews, L. *J. Phys. Chem. A* **1997**, *101*, 5090.